



Supplement of

Global atmospheric carbon monoxide budget 2000–2017 inferred from multi-species atmospheric inversions

Bo Zheng et al.

Correspondence to: Bo Zheng (bo.zheng@lsce.ipsl.fr)

The copyright of individual parts of the supplement might differ from the CC BY 4.0 License.

Table S1. Error settings in the covariance matrices B and R.

Model variable	Error settings	Main reference
Covariance matrix B		
Gridded CO emissions	100% of the largest emission flux in the grid cell within the year	Yin et al. (2015)
Gridded CH ₄ emissions	70% of the largest emission flux among the nine grid cells around	100% in Yin et al. (2015)
Gridded MCF emissions	10%	Yin et al. (2015)
Gridded scaling factors to HCHO produced by NMVOCs	200%	100% in Yin et al. (2015)
Gridded scaling factors to the model initial concentrations of CO, CH ₄ , MCF, and HCHO	10%	Yin et al. (2015)
Scaling factors to the OH fields	5%	10% in Yin et al. (2015)
Covariance matrix R		
CO total column	Instrument errors are from the MOPITT satellite. The forward model and representation errors are estimated as 30% of the measured data.	Yin et al. (2015)
HCHO total column	Instrument errors are from the OMI satellite. The forward model and representation errors are estimated as 30% of the measured data.	Yin et al. (2016)
XCH ₄	Instrument errors are from the GOSAT satellite. The forward model and representation errors are estimated as 10% of the measured data.	Assumed
MCF concentration	Instrument errors are from the WDCGG dataset. The forward model and representation errors are estimated as the standard deviation of detrended and de-seasonalized time series as Yin et al. (2015).	Yin et al. (2015)

Table S2. The WDCGG sites used for evaluating modelled surface CO concentrations.

Site	Contributor	Measurement method	Latitude (°)	Longitude (°)	Measurement altitude (m)	Data period
CGO	AGAGE, CSIRO, NOAA	surface-flask, surface-insitu	-40.68	144.69	164	2000–2017
MHD	AGAGE, NOAA	surface-flask, surface-insitu	53.33	-9.90	5	2000–2017
KVV	ARSO	surface-insitu	46.30	14.53	1750	2005–2017
KOS	CHMI	surface-insitu	49.58	15.08	535	2000–2017 except 2007
CFA	CSIRO	surface-flask	-19.28	147.06	5	2000–2017
CRI	CSIRO	surface-flask	15.08	73.83	66	2000–2002, 2009–2013
CYA	CSIRO	surface-flask	-66.28	110.52	55	2000–2017
ESP	CSIRO	surface-flask	49.38	-126.54	47	2000–2002, 2009–2017
GPA	CSIRO	surface-flask	-12.25	131.05	37	2010–2015
MAA	CSIRO	surface-flask	-67.60	62.87	42	2000–2017
MQA	CSIRO	surface-flask	-54.50	158.94	13	2000–2017
SIS	CSIRO	surface-flask	60.13	-1.18	33	2000–2003
ALT	CSIRO, NOAA	surface-flask	82.50	-62.34	203	2000–2017
MLO	CSIRO, NOAA	surface-flask	19.54	-155.58	3435	2000–2017
SPO	CSIRO, NOAA	surface-flask	-90.00	-24.80	2847	2000–2017
TLL	DMC	surface-insitu	-30.17	-70.80	2159	2013–2015
GAT	DWD	tower-insitu	53.07	11.44	226	2017
CDL	ECCC	surface-insitu	53.99	-105.12	630	2002–2007
CHL	ECCC	surface-insitu	58.74	-93.82	89	2013–2017
CHM	ECCC	surface-insitu	49.69	-74.34	423	2007–2010
EGB	ECCC	surface-insitu	44.23	-79.78	255	2005–2017
ETL	ECCC	surface-insitu	54.35	-104.99	598	2005–2017
FSD	ECCC	surface-insitu	49.84	-81.52	250	2002–2017
WSA	ECCC	surface-insitu	43.93	-60.01	30	2003–2013
JFJ	Empa	surface-insitu	46.55	7.99	3585	2000–2017
PAY	Empa	surface-insitu	46.81	6.94	495	2000–2017
RIG	Empa	surface-insitu	47.07	8.46	1031	2000–2017
CUR	IIA	surface-insitu	39.32	16.42	1801	2014–2017
ABP	INPE, NOAA	surface-flask	-12.77	-38.17	11	2006–2010
BEO	INRNE	surface-insitu	42.18	23.59	2931	2006–2012
CGR	ISAC	surface-insitu	37.67	12.65	9	2015–2017
ECO	ISAC	surface-insitu	40.34	18.12	43	2015,2016
LMT	ISAC	surface-insitu	38.88	16.23	14	2015,2016
MNM	JMA	surface-insitu	24.29	153.98	27	2000–2017 except 2004 and 2005
RYO	JMA	surface-insitu	39.03	141.82	280	2000–2017
YON	JMA	surface-insitu	24.47	123.01	50	2000–2017
PDM	LA	surface-insitu	42.94	0.14	2881	2008–2012
PUY	LAMP	surface-insitu	45.77	2.97	1467	2008–2012
ARH	NIWA	surface-flask	-77.83	166.66	189	2000–2017
BHD	NIWA, NOAA	surface-flask	-41.41	174.87	95	2000–2017
AMT	NOAA	surface-flask	45.03	-68.68	157	2003–2008
AMY	NOAA	surface-flask	36.54	126.33	125	2013–2017
ASC	NOAA	surface-flask	-7.97	-14.40	91	2000–2017
ASK	NOAA	surface-flask	23.27	5.63	2715	2000–2017
AZR	NOAA	surface-flask	38.77	-27.38	24	2000–2017
BAL	NOAA	surface-flask	55.50	16.67	28	2000–2011
BKT	NOAA	surface-flask	-0.20	100.32	875	2001–2017
BME	NOAA	surface-flask	32.37	-64.65	17	2000–2010
BMW	NOAA	surface-flask	32.27	-64.88	30	2000–2017
BRW	NOAA	surface-flask	71.32	-156.61	11	2000–2017

BSC	NOAA	surface-flask	44.17	28.68	5	2000–2011
CBA	NOAA	surface-flask	55.20	-162.72	25	2000–2017 except 2008
CHR	NOAA	surface-flask	1.70	-157.17	3	2000–2017
CPT	NOAA	surface-flask	-34.35	18.49	260	2000–2017
CRZ	NOAA	surface-flask	-46.43	51.83	202	2000–2017
EIC	NOAA	surface-flask	-27.17	-109.42	41	2000–2017
GMI	NOAA	surface-flask	13.43	144.78	2	2000–2017
HBA	NOAA	surface-flask	-75.62	-26.18	35	2000–2017
HPB	NOAA	surface-flask	47.80	11.01	985	2000–2017
HUN	NOAA	surface-flask	46.95	16.65	344	2000–2017
ICE	NOAA	surface-flask	63.40	-20.28	118	2000–2017
IZO	NOAA	surface-flask	28.31	-16.50	2378	2000–2017
KEY	NOAA	surface-flask	25.67	-80.20	6	2000–2017
KUM	NOAA	surface-flask	19.52	-154.82	3	2000–2017
KZD	NOAA	surface-flask	44.45	77.57	412	2000–2009
KZM	NOAA	surface-flask	43.25	77.88	2524	2000–2009
LEF	NOAA	surface-flask	45.93	-90.27	868	2000–2017
LLB	NOAA	surface-flask	54.95	-112.47	548	2007–2017
LLN	NOAA	surface-flask	23.47	120.87	2867	2006–2017
LMP	NOAA	surface-flask	35.52	12.63	50	2006–2017
MEX	NOAA	surface-flask	18.99	-97.31	4469	2009–2017
MID	NOAA	surface-flask	28.22	-177.37	4	2000–2017
MKN	NOAA	surface-flask	-0.06	37.30	3649	2002–2006, 2008–2011
NAT	NOAA	surface-flask	-6.00	-35.20	0	2010–2017
NMB	NOAA	surface-flask	-23.57	15.03	461	2000, 2001, 2006–2017
NWR	NOAA	surface-flask	40.05	-105.59	3526	2000–2017
OXK	NOAA	surface-flask	50.03	11.81	1185	2003, 2006–2017
PAL	NOAA	surface-flask	67.97	24.12	570	2001–2017
PSA	NOAA	surface-flask	-64.77	-64.05	15	2000–2017
PTA	NOAA	surface-flask	38.95	-123.73	22	2000–2011
RPB	NOAA	surface-flask	13.17	-59.43	20	2000–2017
SDZ	NOAA	surface-flask	40.65	117.12	298	2009–2015
SEY	NOAA	surface-flask	-4.67	55.17	3	2000–2017
SGP	NOAA	surface-flask	36.60	-97.50	318	2002–2017
SHM	NOAA	surface-flask	52.72	174.10	28	2000–2017
SMO	NOAA	surface-flask	-14.25	-170.56	77	2000–2017
STM	NOAA	surface-flask	66.00	2.00	4	2000–2009
SUM	NOAA	surface-flask	72.58	-38.48	3215	2000–2017
SYO	NOAA	surface-flask	-69.01	39.58	18	2000–2017
TAP	NOAA	surface-flask	36.73	126.13	21	2000–2017
THD	NOAA	surface-flask	41.05	-124.15	112	2002–2017
TIK	NOAA	surface-flask	71.59	128.92	29	2011–2017
USH	NOAA	surface-flask	-54.85	-68.31	18	2000–2017
UTA	NOAA	surface-flask	39.90	-113.72	1332	2000–2017
UUM	NOAA	surface-flask	44.45	111.10	1012	2000–2017
WIS	NOAA	surface-flask	31.13	34.88	400	2000–2017
WKT	NOAA	surface-flask	31.32	-97.62	723	2001–2010
WLG	NOAA	surface-flask	36.29	100.90	3810	2000–2017
ZEP	NOAA	surface-flask	78.91	11.89	479	2000–2017
TAC	NOAA, UNIVBRIS	surface-flask, surface-insitu	52.52	1.14	196	2012, 2014–2016
KMW	RIVM	surface-insitu	53.33	6.27	4	2000–2012
SNB	UBAA	surface-insitu	47.05	12.96	3111	2002–2017
NGL	UBAG	surface-insitu	53.14	13.03	62	2006–2013
SSL	UBAG	surface-insitu	47.90	7.92	1205	2001–2013
ZSF	UBAG	surface-insitu	47.42	10.98	2671	2007–2017

ZUG	UBAG	surface-insitu	47.42	10.99	2966	2000–2001
GLH	UMLT	surface-insitu	36.07	14.22	174	2000, 2001, 2003, 2004, 2007, 2012–2016
CMN	UNIURB	surface-insitu	44.17	10.68	2172	2007–2017
CVO	UYRK	surface-insitu	16.86	−24.87	20	2008–2016
PDI	VNMHA	surface-insitu	21.57	103.52	1478	2014–2017

Table S3. The TCCON sites used for evaluating modelled column-averaged dry-air mole fractions of CO.

Site	Detectors	Latitude (°)	Longitude (°)	Measurement altitude (m)	Data period	Reference
Indianapolis, IN, USA	xInGaAs Si	39.86	-86.00	270	2012	Iraci et al., 2017a
Manaus, Brazil	xInGaAs Si InSb	-3.21	-60.60	50	2014, 2015	Dubey et al., 2017a
Sodankylä, Finland	xInGaAs Si InSb	67.37	26.63	188	2009–2017	Kivi et al., 2017
Lauder, New Zealand-1	xInGaAs InSb HgCdTe	-45.04	169.68	370	2004–2010	Sherlock et al., 2017a
Lauder, New Zealand-2	xInGaAs Si InSb HgCdTe	-45.04	169.68	370	2010–2017	Sherlock et al., 2017b
Burgos, Philippines	xInGaAs InSb Si	18.53	120.65	35	2017	Morino et al., 2018
Ascension Island	xInGaAs Si	-7.92	-14.33	10	2012–2017	Feist et al., 2017
Réunion Island	xInGaAs Si InSb MCT	-20.90	55.49	87	2011–2017	De Mazière et al., 2017
Caltech, USA	xInGaAs Si InSb	34.14	-118.13	230	2012–2017	Wennberg et al., 2017a
Zugspitze, Germany	xInGaAs Si InSb HgCdTe	47.42	10.98	2960	2015–2017	Sussmann and Rettinger, 2018
Ny Ålesund, Spitsbergen	xInGaAs	78.92	11.92	20	2006–2017	Notholt et al., 2017a
Orléans, France	xInGaAs Si	47.97	2.11	130	2009–2017	Warneke et al., 2017
JPL, Pasadena, CA, USA-1	xInGaAs Si	34.20	-118.18	390	2007, 2008	Wennberg et al., 2017b
JPL, Pasadena, CA, USA-2	xInGaAs Si	34.20	-118.18	390	2011–2017	Wennberg et al., 2017c
Saga, Japan	xInGaAs Si InSb HgCdTe	33.24	130.29	7	2011–2017	Kawakami et al., 2017
Izana, Tenerife	xInGaAs InSb HgCdTe	28.30	-16.48	2370	2007–2017	Blumenstock et al., 2017
Edwards, USA	xInGaAs Si	34.96	-117.88	699	2013–2016	Iraci et al., 2017b
Garmisch, Germany	xInGaAs Si InSb	47.48	11.06	740	2007–2017	Sussmann and Rettinger, 2017
Bremen, Germany	xInGaAs	53.10	8.85	27	2007–2017	Notholt et al., 2017b
Karlsruhe, Germany	xInGaAs InSb	49.10	8.44	116	2010–2017	Hase et al., 2017
Four Corners, USA	xInGaAs Si InSb	36.80	-108.48	1643	2013	Dubey et al., 2017b
Wollongong, Australia	xInGaAs InSb Si	-34.41	150.88	30	2008–2017	Griffith et al., 2017a
East Trout Lake, Canada	xInGaAs InSb	54.36	-104.99	502	2016, 2017	Wunch et al., 2017

Paris, France	xInGaAs InSb HgCdTe	48.85	2.36	60	2014–2017	Té et al., 2017
Anmeyondo, Korea	xInGaAs Si	36.54	126.33	30	2015, 2016	Goo et al., 2017
Park Falls, WI (USA)	xInGaAs Si	45.94	−90.27	440	2004–2017	Wennberg et al., 2017d
Lamont, OK (USA)	xInGaAs Si	36.60	−97.49	320	2008–2017	Wennberg et al., 2017e
Bialystok, Poland	xInGaAs Si	53.23	23.02	180	2009–2017	Deutscher et al., 2017
Rikubetsu, Japan	xInGaAs Si InSb HgCdTe	43.46	143.77	361	2013–2017	Morino et al., 2017a
Eureka, Canada	xInGaAs InSb HgCdTe	80.05	−86.42	610	2010–2017	Strong et al., 2018
Tsukuba, Japan	xInGaAs Si InSb HgCdTe	36.05	140.12	30	2011–2017	Morino et al., 2017b
Darwin, Australia	xInGaAs Si InSb	−12.43	130.89	30	2005–2017	Griffith et al., 2017b

Table S4. Inversion-based estimates of global CO budget from literature. The data unit is Tg CO yr⁻¹.

Study	Constraint	Period ^a	Run ^b	A ^c	BB ^d	O ^e	B ^f	DE ^g	CH ₄ ^h	VOC ⁱ	C ^j	Source ^k	Sink ^l
Müller et al. (2018)	IASI	2013	STD	511	320	98 ^m		929	718	733	1451	2381	
			HN	617	352	107		1076	820	815	1635	2711	
			LN	436	294	91		821	644	674	1318	2139	
			HS	564	354	108		1026	816	813	1629	2655	
			LS	478	293	90		861	648	671	1319	2180	
Jiang et al. (2017)	MOPITT v6	2001–2015	Column Profile Lower profile	499 541 581	287 322 345								
Gaubert et al. (2017)	MOPITT v5	2002–2013	Reanalysis						782	468	1250	2226	
Yin et al. (2015)	MOPITT v6	2002–2011	TransCom INCA					1444 1540			1199 1226	2642 2765	2668 2794
Park et al. (2015)	$\delta^{18}\text{O}$	2004		716	377	20	97	1210	919	454	1373	2583	
Fortems-Cheiney et al. (2012)	OMI, MOPITT v4, WDCGG	2005–2010						1434			1101	2535	2546
Fortems-Cheiney et al. (2011)	MOPITT v4	2000–2009						1412					
Kopacz et al. (2010)	Multiple satellites	MAY 2004 to APR 2005						1350			1507	2857	
Stavrakou and Müller (2006)	MOPITT v3	MAY 2000 to APR 2001	GFED-Grid	664	450	20	199	1333	761	813	1574	2907	
			GFED-Region-Monthly	685	434	20	200	1339	772	794	1566	2905	
			GFED-Region-Annual	675	412	20	186	1293	770	798	1568	2861	
			POET-Grid	688	404	20	195	1307	755	798	1553	2860	
				841	563						394		
Arellano et al. (2006)	MOPITT v3	APR 2000 to MAR 2001											
Arellano et al. (2004)	MOPITT v3	2000	Column	844–	508–				767	175–	2388		
				923	579					209			
			500 mb	782–	531–				767	148–	2363		
				899	633					192			
			700 mb	884–	486–				767	207–	2450		
Pétron et al. (2004)	MOPITT	APR 2000 to MAR 2001		960	573					235			

^a: Year of the data. If data of multiple years are provided, the annual average are presented in the table.

^b: The label of inversion run defined in each paper.

^c: Anthropogenic emissions; ^d: Biomass burning emissions; ^e: Oceanic emissions; ^f: Biogenic emissions; ^g: surface direct emissions from the sum of anthropogenic, biomass burning, oceanic, and biogenic sources; ^h: CO from the oxidation of CH₄; ⁱ: CO from the oxidation of NMVOCs; ^j: chemical production of CO from the sum of CH₄ and NMVOCs oxidation; ^k: CO total source; ^l: CO total sink; ^m: The sum of oceanic and soil emissions are presented in Müller et al. (2018).

Table S5. Global atmospheric carbon monoxide budget during 2000–2017. Average CO budget (10^3 Tg CO yr^{-1}) are derived from Inversions #1, #2, and #3 for the time period of 2000–2017, 2005–2017, and 2010–2017.

Unit: 10^3 Tg CO yr^{-1}	Inv #1	Inv #1	Inv #1	Inv #2	Inv #2	Inv #3
	2000–2017	2005–2017	2010–2017	2005–2017	2010–2017	2010–2017
Sources						
Anthropogenic	0.7	0.7	0.7	0.7	0.7	0.7
Biomass burning	0.5	0.4	0.4	0.4	0.4	0.4
Oceanic	0.02	0.02	0.02	0.02	0.02	0.02
Biogenic	0.2	0.2	0.2	0.2	0.2	0.2
Sub-total direct emissions	1.4	1.3	1.3	1.3	1.3	1.3
Oxidation of CH ₄	0.9	0.9	0.9	0.9	0.9	0.9
Oxidation of NMVOCs	0.3	0.3	0.3	0.3	0.3	0.3
Sub-total chemical production	1.2	1.2	1.2	1.2	1.2	1.2
Total sources	2.6	2.6	2.5	2.6	2.5	2.5
Sinks						
OH reaction	2.6	2.6	2.6	2.6	2.6	2.6

Table S6. Global atmospheric carbon monoxide budget during 2000–2017 estimated using the prior information. Average CO budget (10^3 Tg CO yr^{-1}), coefficient of variation (CV, %), absolute trends from 2000 to 2017 (Tg CO yr^{-2}), and relative trends ($\% \text{ yr}^{-1}$) are all derived from the LMDz-SACS modelling results with the prior information. Absolute and relative trends are both presented with 95% confidence limits. Significant trends are marked by asterisks (* $p < 0.1$, ** $p < 0.05$, and *** $p < 0.01$).

	Average (10^3 Tg CO yr^{-1})	CV (%)	Absolute trend (Tg CO yr^{-2})	Relative trend ($\% \text{ yr}^{-1}$)
Sources				
Anthropogenic	0.6	2.2	$2.0 \pm 0.9^{***}$	$0.33 \pm 0.14^{***}$
Biomass burning	0.3	12.3	-1.2 ± 4.2	-0.43 ± 1.43
Oceanic	0.02	0.1	0.0 ± 0.0	0.00 ± 0.01
Biogenic	0.09	3.3	0.2 ± 0.3	0.21 ± 0.33
Sub-total direct emissions	1.1	3.6	1.0 ± 3.9	0.09 ± 0.39
Oxidation of CH ₄	0.9	1.6	$2.7 \pm 0.3^{***}$	$0.31 \pm 0.04^{***}$
Oxidation of NMVOCs	0.3	0.2	$-0.06 \pm 0.05^{**}$	$-0.02 \pm 0.02^{**}$
Sub-total chemical oxidation	1.2	1.2	$2.6 \pm 0.3^{***}$	$0.22 \pm 0.03^{***}$
Total sources	2.3	1.9	$3.6 \pm 3.8^{*}$	$0.16 \pm 0.18^{*}$
Sinks				
OH reaction	2.3	1.5	2.4 ± 3.2	0.11 ± 0.14

Table S7. Anthropogenic CO emissions and trends during 2000–2017 by region derived from Inversion #1 and Inversion #4. Average anthropogenic CO emissions (Tg CO yr⁻¹), coefficient of variation (CV, %), absolute trends (Tg CO yr⁻²), and relative trends (% yr⁻¹) are estimated for each region on the basis of Inversion #1, Inversion #4, and the prior CEDS inventory. Absolute and relative trends are both presented with 95% confidence limits. Significant trends are marked by asterisks (* $p < 0.1$, ** $p < 0.05$, and *** $p < 0.01$).

	Average (Tg CO yr ⁻¹)	CV (%)	Absolute trend (Inversion #1) (Tg CO yr ⁻²)	Relative trend (Inversion #1) (% yr ⁻¹)	Relative trend (Inversion #4) (% yr ⁻¹)	Average (CEDS) (Tg CO yr ⁻¹)	Absolute trend (CEDS) (Tg CO yr ⁻²)	Relative trend (CEDS) (% yr ⁻¹)
CHN	183.0	6.4	$-1.4 \pm 0.9^{***}$	$-0.77 \pm 0.49^{***}$	$-1.33 \pm 0.44^{***}$	185.8	$2.2 \pm 0.7^{***}$	$1.31 \pm 0.44^{***}$
SAS	83.6	7.4	$0.8 \pm 0.5^{***}$	$1.01 \pm 0.64^{***}$	0.16 ± 0.66	84.8	$2.3 \pm 0.3^{***}$	$3.51 \pm 0.40^{***}$
USA	69.9	26.8	$-3.4 \pm 0.6^{***}$	$-3.01 \pm 0.53^{***}$	$-2.16 \pm 0.61^{***}$	59.5	$-3.1 \pm 0.5^{***}$	$-3.26 \pm 0.56^{***}$
EQAF	64.9	10.8	$1.1 \pm 0.4^{***}$	$2.01 \pm 0.72^{***}$	$1.37 \pm 0.57^{***}$	45.9	$0.8 \pm 0.1^{***}$	$2.06 \pm 0.25^{***}$
EU	53.7	18.0	$-1.6 \pm 0.5^{***}$	$-2.41 \pm 0.74^{***}$	$-1.10 \pm 0.83^{**}$	28.9	$-1.0 \pm 0.1^{***}$	$-2.62 \pm 0.35^{***}$
SEAS	43.8	25.3	-0.2 ± 1.1	-0.45 ± 2.04	-0.01 ± 1.85	56.3	$1.3 \pm 0.2^{***}$	$3.01 \pm 0.38^{***}$
MIDE	37.3	16.8	-0.4 ± 0.6	-1.09 ± 1.54	0.54 ± 1.49	18.6	-0.05 ± 0.1	-0.31 ± 0.61
NAF	31.2	14.6	$0.7 \pm 0.3^{***}$	$2.81 \pm 1.16^{***}$	$2.39 \pm 0.66^{***}$	19.6	$0.4 \pm 0.1^{***}$	$2.02 \pm 0.34^{***}$
RUS	28.3	20.3	-0.4 ± 0.6	-1.25 ± 1.74	$-1.65 \pm 1.68^{*}$	11.6	$-0.3 \pm 0.0^{***}$	$-2.04 \pm 0.25^{***}$
SAF	27.6	12.3	$0.3 \pm 0.3^{*}$	$0.84 \pm 1.00^{*}$	0.85 ± 1.04	15.7	$0.1 \pm 0.0^{***}$	$0.78 \pm 0.14^{***}$
BRA	27.0	9.0	-0.1 ± 0.2	-0.32 ± 0.76	$-0.70 \pm 0.78^{*}$	15.8	$-0.05 \pm 0.06^{*}$	$-0.33 \pm 0.36^{*}$
SSA	11.8	21.9	-0.02 ± 0.3	-0.10 ± 1.45	$-2.01 \pm 1.37^{***}$	9.0	$0.2 \pm 0.1^{***}$	$2.03 \pm 0.59^{***}$
KAJ	11.7	23.8	$-0.5 \pm 0.2^{***}$	$-3.02 \pm 0.97^{***}$	$-1.59 \pm 0.85^{***}$	13.3	$-0.4 \pm 0.0^{***}$	$-2.24 \pm 0.22^{***}$
CAS	11.5	16.5	0.03 ± 0.2	0.34 ± 2.26	1.03 ± 1.86	5.4	$0.05 \pm 0.04^{**}$	$1.12 \pm 0.83^{**}$
CAM	11.5	32.0	$-0.4 \pm 0.3^{***}$	$-2.09 \pm 1.40^{***}$	$-1.96 \pm 1.34^{***}$	18.3	$-0.2 \pm 0.0^{***}$	$-0.83 \pm 0.17^{***}$
CAN	9.6	39.6	0.2 ± 0.4	2.03 ± 3.36	$-4.09 \pm 2.25^{***}$	5.8	$-0.2 \pm 0.0^{***}$	$-2.78 \pm 0.38^{***}$
NSA	8.6	13.7	-0.01 ± 0.1	-0.07 ± 1.22	-0.89 ± 1.15	11.3	0.01 ± 0.06	0.11 ± 0.56
OCE	8.0	28.6	-0.1 ± 0.2	-1.21 ± 2.69	-0.98 ± 1.75	3.9	$-0.03 \pm 0.02^{***}$	$-0.82 \pm 0.47^{***}$

Table S8. Anthropogenic CO emissions and trends during 2005–2017 by region derived from Inversion #2. Average anthropogenic CO emissions (Tg CO yr^{-1}), coefficient of variation (CV, %), absolute trends (Tg CO yr^{-2}), and relative trends ($\% \text{ yr}^{-1}$) are estimated for each region on the basis of Inversion #2 and the prior CEDS inventory. Absolute and relative trends are both presented with 95% confidence limits. Significant trends are marked by asterisks (* $p < 0.1$, ** $p < 0.05$, and *** $p < 0.01$).

	Average (Tg CO yr^{-1})	CV (%)	Absolute trend (Inversion #2) (Tg CO yr^{-2})	Relative trend (Inversion #2) ($\% \text{ yr}^{-1}$)	Average (CEDS) (Tg CO yr^{-1})	Absolute trend (CEDS) (Tg CO yr^{-2})	Relative trend (CEDS) ($\% \text{ yr}^{-1}$)
CHN	176.2	10.5	$-4.1 \pm 1.9^{***}$	$-2.04 \pm 0.94^{***}$	193.4	$0.9 \pm 0.9^*$	$0.48 \pm 0.49^*$
SAS	85.9	5.2	0.0 ± 0.8	0.01 ± 0.90	90.9	$2.0 \pm 0.5^{***}$	$2.66 \pm 0.62^{***}$
USA	61.1	22.8	$-3.4 \pm 1.0^{***}$	$-3.96 \pm 1.11^{***}$	50.5	$-2.2 \pm 0.6^{***}$	$-3.15 \pm 0.89^{***}$
EQAF	69.7	6.3	$0.8 \pm 0.6^{**}$	$1.14 \pm 0.91^{**}$	47.9	$0.9 \pm 0.2^{***}$	$2.13 \pm 0.43^{***}$
EU	53.7	23.3	$-2.2 \pm 1.6^{**}$	$-3.45 \pm 2.53^{**}$	26.0	$-0.8 \pm 0.2^{***}$	$-2.41 \pm 0.56^{***}$
SEAS	30.7	54.7	0.0 ± 3.0	0.07 ± 7.58	60.1	$1.1 \pm 0.3^{***}$	$2.10 \pm 0.51^{***}$
MIDE	41.6	28.9	$-1.6 \pm 1.9^*$	$-3.62 \pm 4.23^*$	18.8	$-0.3 \pm 0.1^{***}$	$-1.41 \pm 0.38^{***}$
NAF	36.0	18.3	0.2 ± 1.2	0.87 ± 4.07	20.5	$0.4 \pm 0.1^{***}$	$2.11 \pm 0.63^{***}$
RUS	28.0	20.9	-0.3 ± 1.0	-0.87 ± 3.20	10.8	$-0.3 \pm 0.1^{***}$	$-2.00 \pm 0.48^{***}$
SAF	29.1	14.6	-0.1 ± 0.7	-0.50 ± 3.02	16.0	$0.1 \pm 0.0^{***}$	$0.90 \pm 0.26^{***}$
BRA	28.9	11.6	-0.2 ± 0.6	-0.92 ± 2.10	15.7	$-0.1 \pm 0.1^{***}$	$-0.85 \pm 0.41^{***}$
SSA	13.2	19.4	0.0 ± 0.5	0.30 ± 3.59	9.4	$0.2 \pm 0.1^{***}$	$2.76 \pm 0.97^{***}$
KAJ	9.4	32.6	$-0.5 \pm 0.4^{**}$	$-3.22 \pm 3.05^{**}$	12.5	$-0.4 \pm 0.1^{***}$	$-2.62 \pm 0.42^{***}$
CAS	12.1	23.8	-0.3 ± 0.5	-1.88 ± 3.04	5.6	0.0 ± 0.1	-0.25 ± 1.12
CAM	4.0	150.8	0.4 ± 1.0	8.05 ± 19.37	17.8	$-0.1 \pm 0.0^{***}$	$-0.55 \pm 0.16^{***}$
CAN	12.0	41.9	0.4 ± 0.9	4.93 ± 10.19	5.1	$-0.2 \pm 0.0^{***}$	$-2.64 \pm 0.63^{***}$
NSA	5.1	63.2	0.2 ± 0.6	2.83 ± 9.80	11.4	-0.1 ± 0.1	-0.60 ± 0.96
OCE	8.5	25.2	$-0.4 \pm 0.3^{**}$	$-4.33 \pm 3.15^{**}$	3.8	$-0.1 \pm 0.0^{***}$	$-1.47 \pm 0.4^{***}$

Table S9. Anthropogenic CO emissions and trends during 2010–2017 by region derived from Inversion #3. Average anthropogenic CO emissions (Tg CO yr^{-1}), coefficient of variation (CV, %), absolute trends (Tg CO yr^{-2}), and relative trends ($\% \text{ yr}^{-1}$) are estimated for each region on the basis of Inversion #3 and the prior CEDS inventory. Absolute and relative trends are both presented with 95% confidence limits. Significant trends are marked by asterisks (* $p < 0.1$, ** $p < 0.05$, and *** $p < 0.01$).

	Average (Tg CO yr^{-1})	CV (%)	Absolute trend (Inversion #3) (Tg CO yr^{-2})	Relative trend (Inversion #3) ($\% \text{ yr}^{-1}$)	Average (CEDS) (Tg CO yr^{-1})	Absolute trend (CEDS) (Tg CO yr^{-2})	Relative trend (CEDS) ($\% \text{ yr}^{-1}$)
CHN	162.2	9.2	-3.7 ± 5.3	-2.23 ± 3.16	195.5	$-0.3 \pm 0.3^*$	$-0.14 \pm 0.17^*$
SAS	87.4	4.2	$-1.1 \pm 1.2^*$	$-1.17 \pm 1.31^*$	96.6	$0.9 \pm 0.3^{***}$	$0.94 \pm 0.36^{***}$
USA	53.2	13.4	$-2.2 \pm 2.2^*$	$-3.9 \pm 4.0^*$	44.6	$-1.0 \pm 0.4^{***}$	$-2.01 \pm 0.83^{***}$
EQAF	73.3	5.9	0.9 ± 1.6	1.24 ± 2.24	50.4	$0.5 \pm 0.3^{***}$	$0.99 \pm 0.61^{***}$
EU	50.6	17.2	-1.6 ± 3.4	-2.88 ± 6.00	23.9	$-0.5 \pm 0.3^{***}$	$-1.74 \pm 1.02^{***}$
SEAS	30.9	27.7	-0.6 ± 3.7	-1.61 ± 10.74	62.9	$0.6 \pm 0.3^{***}$	$0.92 \pm 0.50^{***}$
MIDE	40.8	25.6	-2.3 ± 4.0	-4.20 ± 7.32	17.9	$-0.1 \pm 0.1^{**}$	$-0.66 \pm 0.52^{**}$
NAF	38.7	12.8	-0.6 ± 2.1	-1.36 ± 5.14	21.5	$0.2 \pm 0.1^{***}$	$0.77 \pm 0.38^{***}$
RUS	28.8	18.7	-0.6 ± 2.3	-1.49 ± 6.06	10.1	$-0.1 \pm 0.0^{***}$	$-1.15 \pm 0.46^{***}$
SAF	29.6	10.9	-0.7 ± 1.2	-1.89 ± 3.26	16.3	$0.2 \pm 0.1^{***}$	$1.15 \pm 0.72^{***}$
BRA	28.6	7.1	0.2 ± 0.9	0.84 ± 3.33	15.3	$0.0 \pm 0.0^{**}$	$-0.16 \pm 0.16^{**}$
SSA	13.3	22.5	-0.4 ± 1.2	-3.09 ± 8.62	10.0	$0.1 \pm 0.0^{**}$	$0.57 \pm 0.51^{**}$
KAJ	7.9	19.5	-0.1 ± 0.7	-1.31 ± 8.48	11.4	$-0.3 \pm 0.1^{***}$	$-2.14 \pm 1.06^{***}$
CAS	11.3	16.8	-0.1 ± 0.8	-1.00 ± 5.64	5.5	0.0 ± 0.0	-0.34 ± 0.63
CAM	4.1	102.9	-0.1 ± 1.9	-11.33 ± 281.09	17.5	$-0.1 \pm 0.1^{**}$	$-0.35 \pm 0.35^{**}$
CAN	12.6	35.4	0.7 ± 1.8	6.07 ± 16.29	4.6	$-0.1 \pm 0.1^{**}$	$-1.81 \pm 1.30^{**}$
NSA	4.8	62.8	0.1 ± 1.3	2.19 ± 24.06	11.3	$-0.2 \pm 0.2^{**}$	$-1.82 \pm 1.65^{**}$
OCE	8.1	20.7	$-0.5 \pm 0.6^*$	$-6.02 \pm 6.98^*$	3.7	$0.0 \pm 0.0^{***}$	$-1.24 \pm 0.51^{***}$

Table S10. Biomass burning CO emissions and trends during 2000–2017 by region derived from Inversion #1 and Inversion #4. Average biomass burning CO emissions (Tg CO yr⁻¹), coefficient of variation (CV, %), absolute trends (Tg CO yr⁻²), and relative trends (% yr⁻¹) are estimated for each region on the basis of Inversion #1, Inversion #4, and the prior GFED 4.1s inventory. Absolute and relative trends are both presented with 95% confidence limits. Significant trends are marked by asterisks (* $p < 0.1$, ** $p < 0.05$, and *** $p < 0.01$).

	Average (Tg CO yr ⁻¹)	CV (%)	Absolute trend (Inversion #1) (Tg CO yr ⁻²)	Relative trend (Inversion #1) (% yr ⁻¹)	Relative trend (Inversion #4) (% yr ⁻¹)	Average (GFED) (Tg CO yr ⁻¹)	Absolute trend (GFED 4.1s) (Tg CO yr ⁻²)	Relative trend (GFED 4.1s) (% yr ⁻¹)
EQAF	92.6	14.2	$-1.6 \pm 1.1^{***}$	$-1.47 \pm 0.99^{***}$	$-1.08 \pm 0.85^{**}$	74.7	$-1.1 \pm 0.5^{***}$	$-1.27 \pm 0.55^{***}$
SAF	82.8	10.0	-0.2 ± 0.8	-0.25 ± 1.05	-0.26 ± 0.78	55.0	0.0 ± 0.4	0.00 ± 0.79
BRA	58.8	43.8	-0.4 ± 2.6	-1.10 ± 7.57	-1.37 ± 4.70	33.9	-0.1 ± 1.8	-0.53 ± 9.97
SEAS	50.1	59.5	-0.2 ± 3.0	-0.57 ± 11.47	-1.34 ± 5.62	47.1	0.5 ± 3.4	2.31 ± 16.14
RUS	37.5	37.4	-0.1 ± 1.4	-0.40 ± 4.43	-1.27 ± 2.68	34.4	-0.4 ± 1.6	-1.16 ± 4.96
OCE	28.4	37.9	$-0.9 \pm 1.0^*$	$-2.23 \pm 2.43^*$	-1.53 ± 2.74	15.5	$-0.4 \pm 0.5^*$	$-2.52 \pm 2.85^*$
NAF	27.2	10.0	0.01 ± 0.28	0.02 ± 1.03	-0.02 ± 0.91	20.9	-0.1 ± 0.2	-0.52 ± 0.64
SSA	18.9	52.2	-0.7 ± 0.9	-2.69 ± 3.64	$-2.94 \pm 2.59^{**}$	11.1	-0.2 ± 0.5	-1.93 ± 4.39
CAN	14.2	47.6	$0.8 \pm 0.6^{**}$	$11.00 \pm 8.34^{**}$	1.78 ± 4.09	14.7	$0.8 \pm 0.7^{**}$	$15.17 \pm 12.66^{**}$
USA	6.7	45.4	0.1 ± 0.3	1.87 ± 6.19	$2.80 \pm 3.17^*$	6.0	0.1 ± 0.4	1.29 ± 9.38
CAM	6.3	56.9	-0.3 ± 0.3	-1.98 ± 2.57	-1.07 ± 2.04	5.3	-0.1 ± 0.2	-1.47 ± 2.55
CAS	5.4	57.8	-0.2 ± 0.3	-6.29 ± 7.70	$-3.56 \pm 3.22^{**}$	3.1	-0.1 ± 0.2	-5.43 ± 7.48
EU	4.7	25.4	$-0.1 \pm 0.1^{**}$	$-1.48 \pm 1.45^{**}$	-0.74 ± 1.42	2.4	$-0.06 \pm 0.06^{**}$	$-1.63 \pm 1.62^{**}$
NSA	3.8	43.4	-0.1 ± 0.2	-2.16 ± 3.04	-2.32 ± 2.86	3.8	-0.08 ± 0.12	-1.63 ± 2.53
CHN	3.7	18.7	0.04 ± 0.07	1.14 ± 1.75	0.92 ± 1.59	3.7	$0.1 \pm 0.1^{**}$	$3.07 \pm 2.41^{**}$
SAS	2.5	30.3	0.04 ± 0.07	1.43 ± 2.82	0.87 ± 2.36	2.1	$0.06 \pm 0.06^{**}$	$3.42 \pm 3.03^{**}$
MIDE	0.9	29.8	0.00 ± 0.03	0.21 ± 3.04	1.76 ± 3.03	0.3	0.00 ± 0.01	1.51 ± 3.21
KAJ	0.3	39.8	$-0.01 \pm 0.01^{**}$	$-2.51 \pm 2.17^{**}$	-0.64 ± 1.58	0.3	-0.01 ± 0.01	-1.78 ± 2.17

Table S11. Biomass burning CO emissions and trends during 2005–2017 by region derived from Inversion #2. Average biomass burning CO emissions (Tg CO yr⁻¹), coefficient of variation (CV, %), absolute trends (Tg CO yr⁻²), and relative trends (% yr⁻¹) are estimated for each region on the basis of Inversion #2 and the prior GFED 4.1s inventory. Absolute and relative trends are both presented with 95% confidence limits. Significant trends are marked by asterisks (* $p < 0.1$, ** $p < 0.05$, and *** $p < 0.01$).

	Average (Tg CO yr ⁻¹)	CV (%)	Absolute trend (Inversion #2) (Tg CO yr ⁻²)	Relative trend (Inversion #2) (% yr ⁻¹)	Average (GFED 4.1s) (Tg CO yr ⁻¹)	Absolute trend (GFED 4.1s) (Tg CO yr ⁻²)	Relative trend (GFED 4.1s) (% yr ⁻¹)
EQAF	85.3	12.4	-0.7 ± 1.8	-0.71 ± 1.73	71.7	$-0.8 \pm 0.8^*$	$-0.95 \pm 0.96^*$
SAF	83.7	13.1	-1.0 ± 1.8	-1.17 ± 2.05	55.5	-0.3 ± 0.4	-0.58 ± 0.76
BRA	59.2	43.8	-1.8 ± 4.4	-1.81 ± 4.50	35.4	-1.5 ± 3.4	-2.47 ± 5.62
SEAS	45.6	59.8	-0.6 ± 4.8	-1.48 ± 11.14	49.1	-0.6 ± 6.3	-1.35 ± 15.51
RUS	35.9	34.5	0.5 ± 2.2	1.76 ± 7.58	32.2	0.3 ± 2.1	1.62 ± 9.86
OCE	25.5	42.3	-0.5 ± 1.9	-2.97 ± 11.84	13.8	0.0 ± 0.9	-0.36 ± 8.92
NAF	27.6	10.2	-0.2 ± 0.5	-0.53 ± 1.62	20.6	-0.1 ± 0.3	-0.58 ± 1.04
SSA	18.0	47.5	-1.0 ± 1.4	-4.14 ± 5.49	10.8	-0.5 ± 0.9	-3.44 ± 5.56
CAN	16.1	51.8	$1.2 \pm 1.2^*$	$11.78 \pm 12.07^*$	15.9	$1.2 \pm 1.1^{**}$	$10.55 \pm 10.00^{**}$
USA	7.0	38.5	0.0 ± 0.5	0.31 ± 4.85	5.9	0.0 ± 0.6	0.15 ± 5.36
CAM	4.9	54.7	-0.2 ± 0.4	-2.35 ± 4.36	5.0	-0.2 ± 0.3	-2.07 ± 3.27
CAS	5.2	42.7	$-0.3 \pm 0.3^*$	$-4.83 \pm 5.18^*$	2.8	$-0.2 \pm 0.2^*$	$-6.88 \pm 8.18^*$
EU	5.1	29.4	-0.1 ± 0.3	-1.99 ± 4.50	2.3	-0.1 ± 0.1	-1.91 ± 3.40
NSA	2.2	62.7	0.1 ± 0.2	3.41 ± 8.79	3.4	0.0 ± 0.2	0.38 ± 5.28
CHN	3.7	16.0	0.0 ± 0.1	-0.26 ± 2.87	4.0	0.1 ± 0.1	2.27 ± 4.08
SAS	2.6	31.6	0.0 ± 0.1	-0.30 ± 5.84	2.3	0.0 ± 0.1	2.11 ± 5.64
MIDE	1.1	40.4	0.0 ± 0.1	-1.85 ± 8.70	0.3	0.0 ± 0.0	2.21 ± 5.75
KAJ	0.2	30.0	0.0 ± 0.0	-1.58 ± 2.90	0.3	0.0 ± 0.0	-0.26 ± 2.33

Table S12. Biomass burning CO emissions and trends during 2010–2017 by region derived from Inversion #3. Average biomass burning CO emissions (Tg CO yr^{-1}), coefficient of variation (CV, %), absolute trends (Tg CO yr^{-2}), and relative trends ($\% \text{ yr}^{-1}$) are estimated for each region on the basis of Inversion #3 and the prior GFED 4.1s inventory. Absolute and relative trends are both presented with 95% confidence limits. Significant trends are marked by asterisks (* $p < 0.1$, ** $p < 0.05$, and *** $p < 0.01$).

	Average (Tg CO yr^{-1})	CV (%)	Absolute trend (Inversion #3) (Tg CO yr^{-2})	Relative trend (Inversion #3) ($\% \text{ yr}^{-1}$)	Average (GFED 4.1s) (Tg CO yr^{-1})	Absolute trend (GFED 4.1s) (Tg CO yr^{-2})	Relative trend (GFED 4.1s) ($\% \text{ yr}^{-1}$)
EQAF	83.9	9.5	1.7 ± 3.0	2.12 ± 3.73	69.1	0.2 ± 1.7	0.34 ± 2.42
SAF	84.6	11.7	$-3.0 \pm 3.1^*$	$-2.86 \pm 2.94^*$	55.3	$-1.2 \pm 0.8^{**}$	$-1.92 \pm 1.28^{**}$
BRA	55.3	37.2	1.3 ± 8.9	1.52 ± 10.72	33.4	-1.6 ± 6.9	-2.32 ± 10.03
SEAS	43.5	69.7	0.4 ± 13.2	1.27 ± 42.87	46.1	2.3 ± 15.4	8.87 ± 60.58
RUS	35.7	27.3	-0.6 ± 4.2	-1.58 ± 11.77	33.5	-0.4 ± 5.0	-1.69 ± 19.04
OCE	26.1	48.9	-1.6 ± 5.3	-12.70 ± 43.73	14.0	-0.4 ± 2.3	-7.34 ± 39.81
NAF	27.4	9.9	0.4 ± 1.1	1.64 ± 4.93	20.1	0.2 ± 0.4	1.17 ± 2.02
SSA	17.6	55.2	$-3.1 \pm 2.9^{**}$	$-7.75 \pm 7.42^{**}$	10.4	-1.3 ± 2.1	-5.44 ± 8.47
CAN	19.0	45.8	1.1 ± 3.7	8.57 ± 29.41	20.0	0.5 ± 3.0	2.90 ± 16.45
USA	7.0	42.1	0.5 ± 1.2	9.98 ± 23.95	5.6	0.5 ± 1.3	11.90 ± 31.11
CAM	4.5	58.0	-0.3 ± 1.1	-10.83 ± 39.51	4.6	0.0 ± 0.7	-1.01 ± 21.42
CAS	4.1	48.5	0.0 ± 0.9	-0.48 ± 14.44	2.2	0.0 ± 0.5	1.12 ± 19.70
EU	5.0	30.2	0.0 ± 0.7	1.24 ± 17.63	2.1	0.1 ± 0.2	6.00 ± 12.26
NSA	2.2	65.4	0.2 ± 0.6	7.69 ± 22.63	3.3	0.1 ± 0.4	3.59 ± 10.28
CHN	3.6	24.0	0.0 ± 0.4	0.22 ± 11.14	4.1	0.1 ± 0.4	2.69 ± 10.37
SAS	2.6	26.3	0.0 ± 0.3	-1.41 ± 10.00	2.3	0.0 ± 0.2	1.05 ± 9.00
MIDE	1.2	39.4	-0.1 ± 0.2	-4.40 ± 9.27	0.4	0.0 ± 0.0	-0.57 ± 9.46
KAJ	0.2	26.9	0.0 ± 0.0	7.44 ± 20.37	0.3	0.0 ± 0.0	3.52 ± 8.62

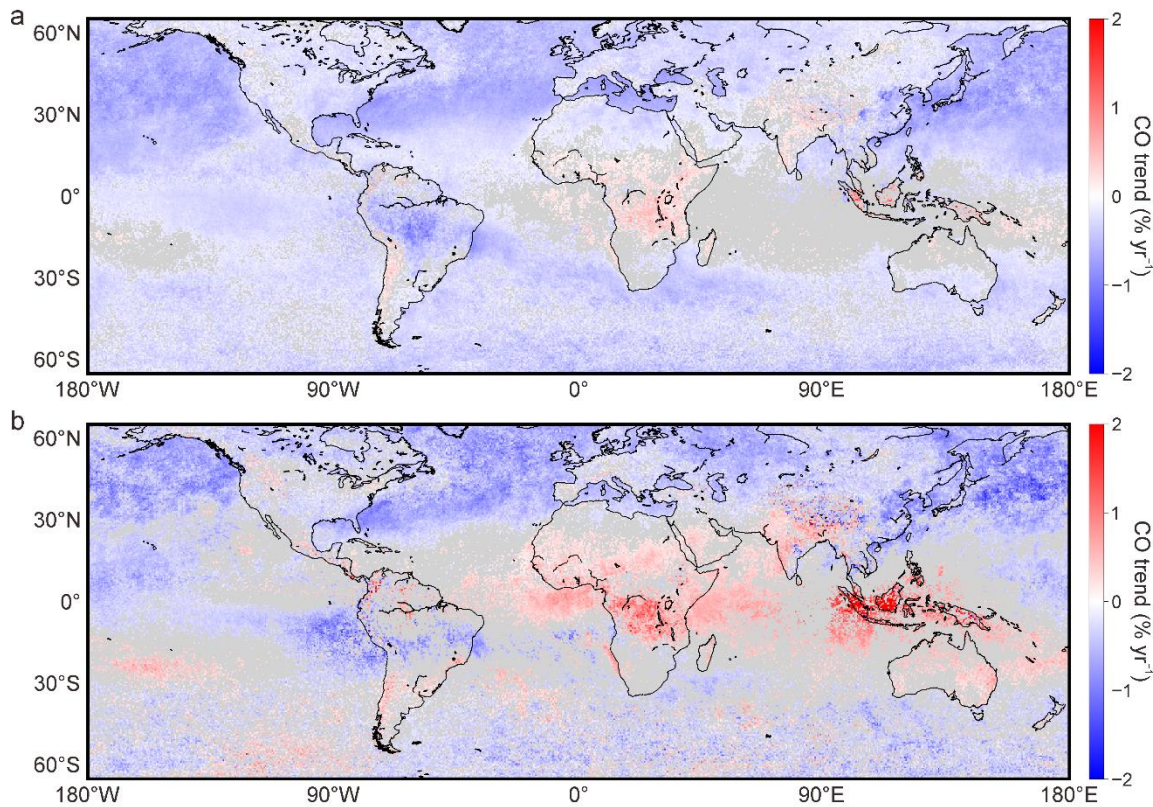


Figure S1. Trends in the MOPITT CO columns. The map (a) shows the 2005–2017 trends in MOPITT CO total columns at the spatial resolution of $0.5^\circ \times 0.5^\circ$, and the map (b) shows the trends from 2010 to 2017. The trends in (a) and (b) are both estimated on the base of monthly time series using a curve fitting method as described in Zheng et al. (2018). The grey colour in maps indicates the areas without statistically significant trends ($p \geq 0.05$).

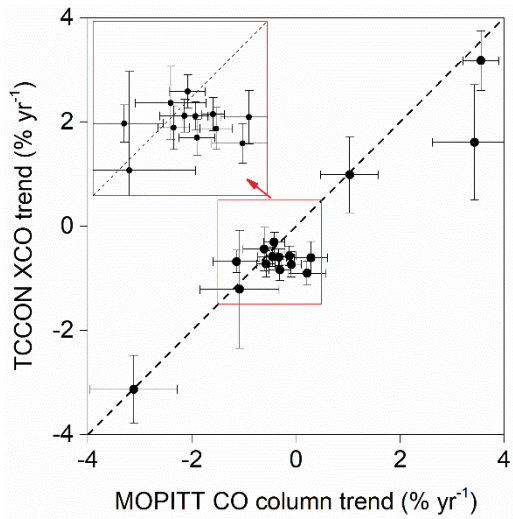


Figure S2. Comparison between the trends of MOPITT CO column and TCCON XCO. Each dot represents a site in TCCON archive plotted according to the observed XCO trend (y-axis) and the collocated CO column trend derived from MOPITT v7 retrievals (x-axis). These TCCON sites all present statistically significant trends ($p < 0.05$) with the error bars being 95% confidence intervals. The MOPITT
5 CO columns are first averaged to generate monthly global maps at the spatial resolution of $0.5^\circ \times 0.5^\circ$, and then the grid cells that contain the TCCON sites are used in the comparison with TCCON observations. The trends shown in this figure are calculated based on monthly time series using a curve fitting method as described in Zheng et al. (2018).

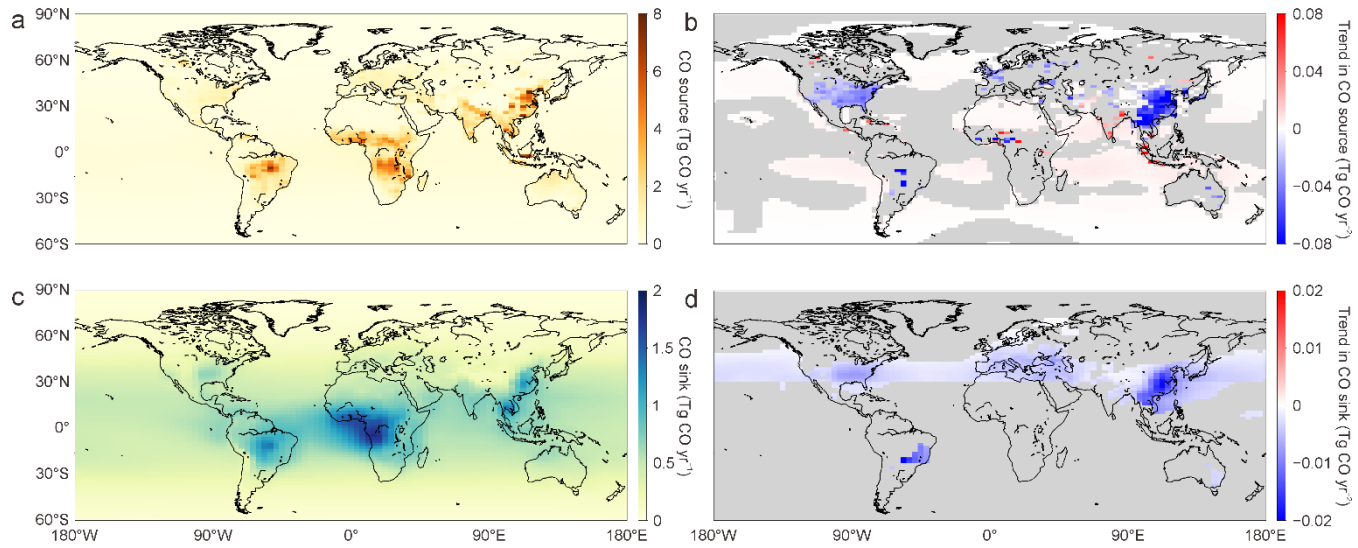


Figure S3. Spatial distribution of the global CO budget and 2005–2017 trends. Annual average CO total source and sink during 2005–2017 are shown at the spatial resolution of 3.75° longitude $\times 1.9^\circ$ latitude in (a) and (c), respectively, and linear trends of each grid cell are shown in (b) and (d), which are estimated using the linear least squares fitting method based on annual time series. Grey colour in (b) and (d) indicates the areas without statistically significant trends ($p \geq 0.05$). All data shown in this figure are derived from Inversion #2 results.

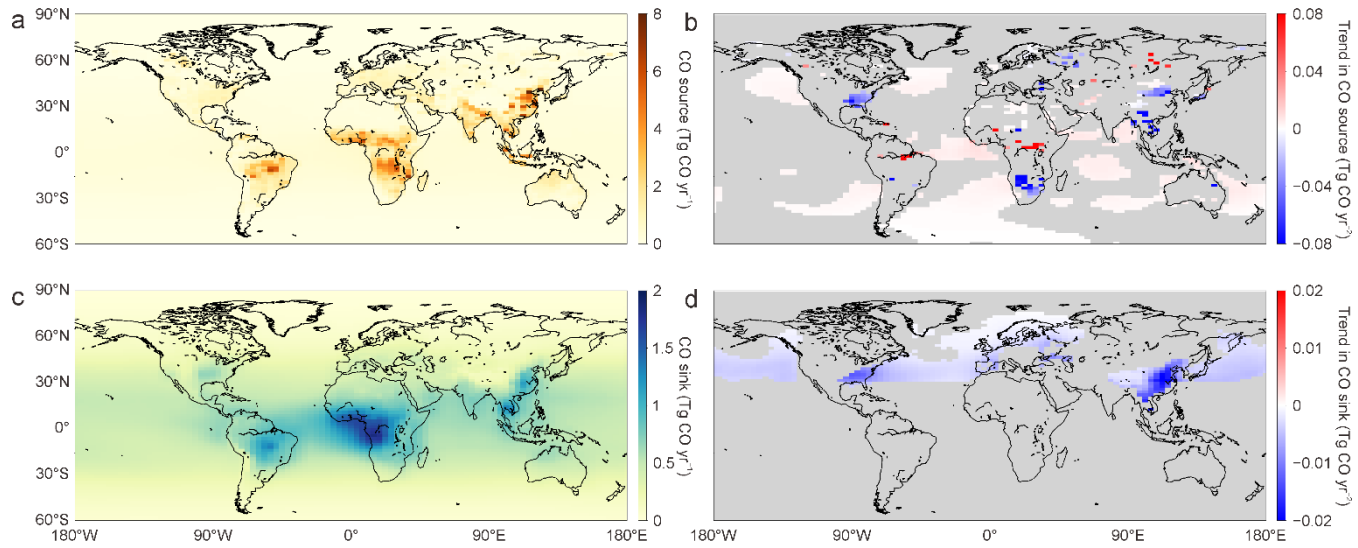
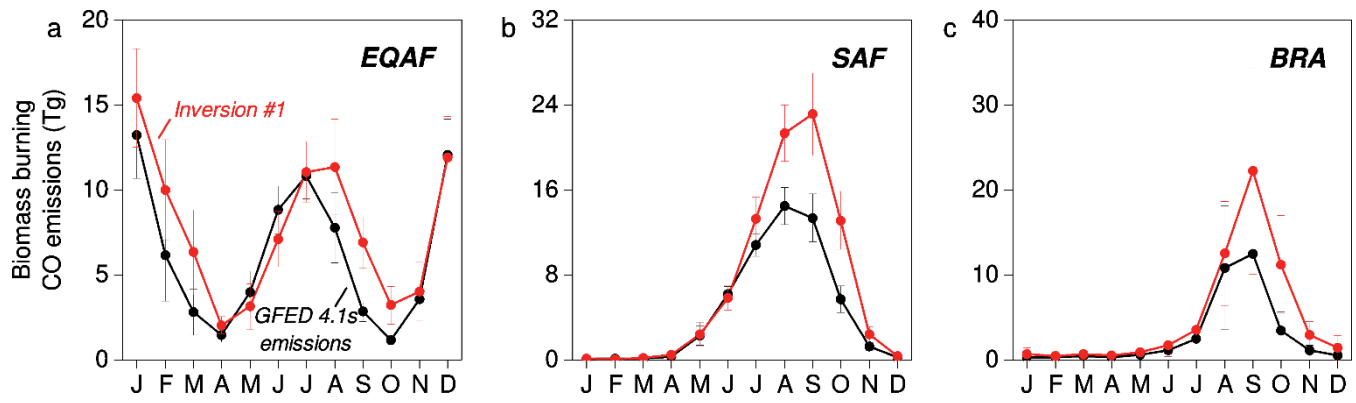


Figure S4. Spatial distribution of the global CO budget and 2010–2017 trends. Annual average CO total source and sink during 2010–2017 are shown at the spatial resolution of 3.75° longitude $\times 1.9^\circ$ latitude in (a) and (c), respectively, and linear trends of each grid cell are shown in (b) and (d), which are estimated using the linear least squares fitting method based on annual time series. Grey colour in (b) and (d) indicates the areas without statistically significant trends ($p \geq 0.05$). All data shown in this figure are derived from Inversion #3 results.



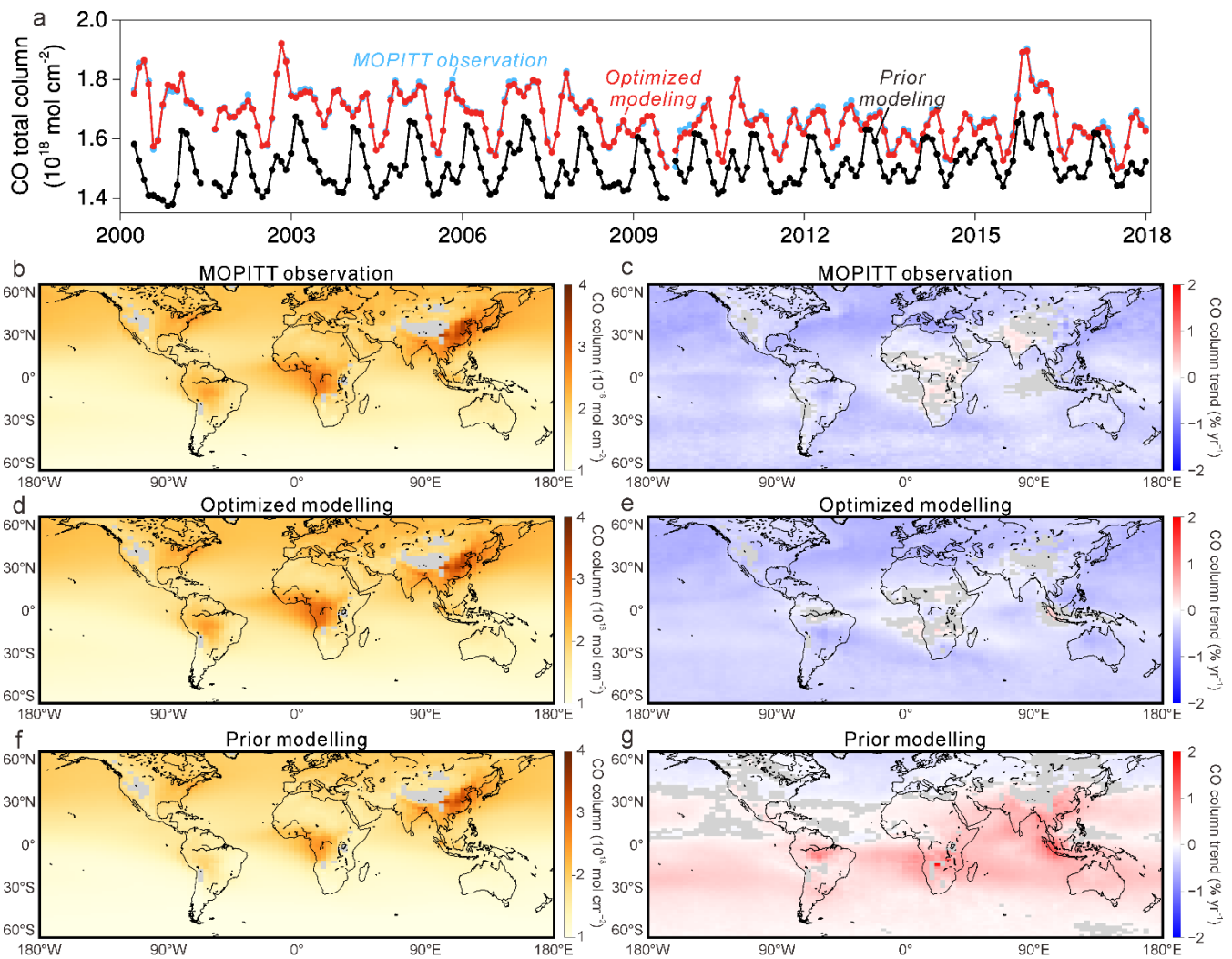


Figure S6. Evaluation of modelled CO total columns with MOPITT observations. Global monthly average CO total columns are presented in (a) with MOPITT observations (blue curve), modelling with prior emissions (black curve), and modelling with Inversion #1 optimized emissions (red curve). Annual average CO total columns are presented at the spatial resolution of $3.75^\circ \text{ longitude} \times 1.9^\circ \text{ latitude}$ for MOPITT observations (b), Inversion #1 modelling (d), and the prior modelling (f). Trends in CO total columns during 2000–2017 are presented at the spatial resolution of $3.75^\circ \text{ longitude} \times 1.9^\circ \text{ latitude}$ for MOPITT observations (c), Inversion #1 modelling (e), and the prior modelling (g). The trends in (c), (e), and (g) are estimated on the base of monthly time series using a curve fitting method as described in Zheng et al. (2018). Grey colour in all of the maps indicates the areas without valid data or statistically significant trends ($p \geq 0.05$).
5

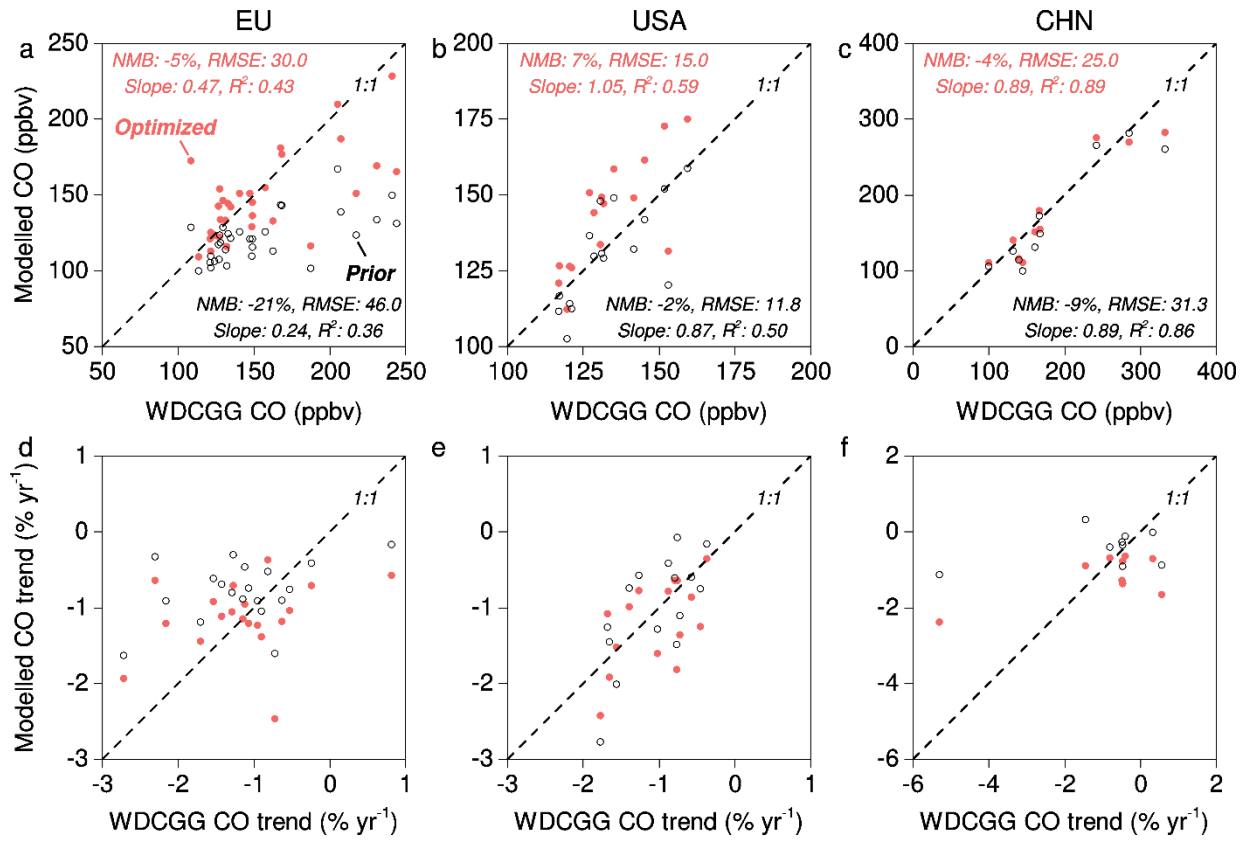


Figure S7. Evaluation of Inversion #1 with the WDCGG observations by region. The comparison is conducted for annual average and 2000–2017 trends of surface CO concentrations between the modelled results and the WDCGG observations in EU (a, d), the USA (b, e), and CHN (c, f). The WDCGG sites used for each region are within the three black boxes shown in Fig. A1. The trends are calculated based on monthly time series using a curve fitting method as described in Zheng et al. (2018).

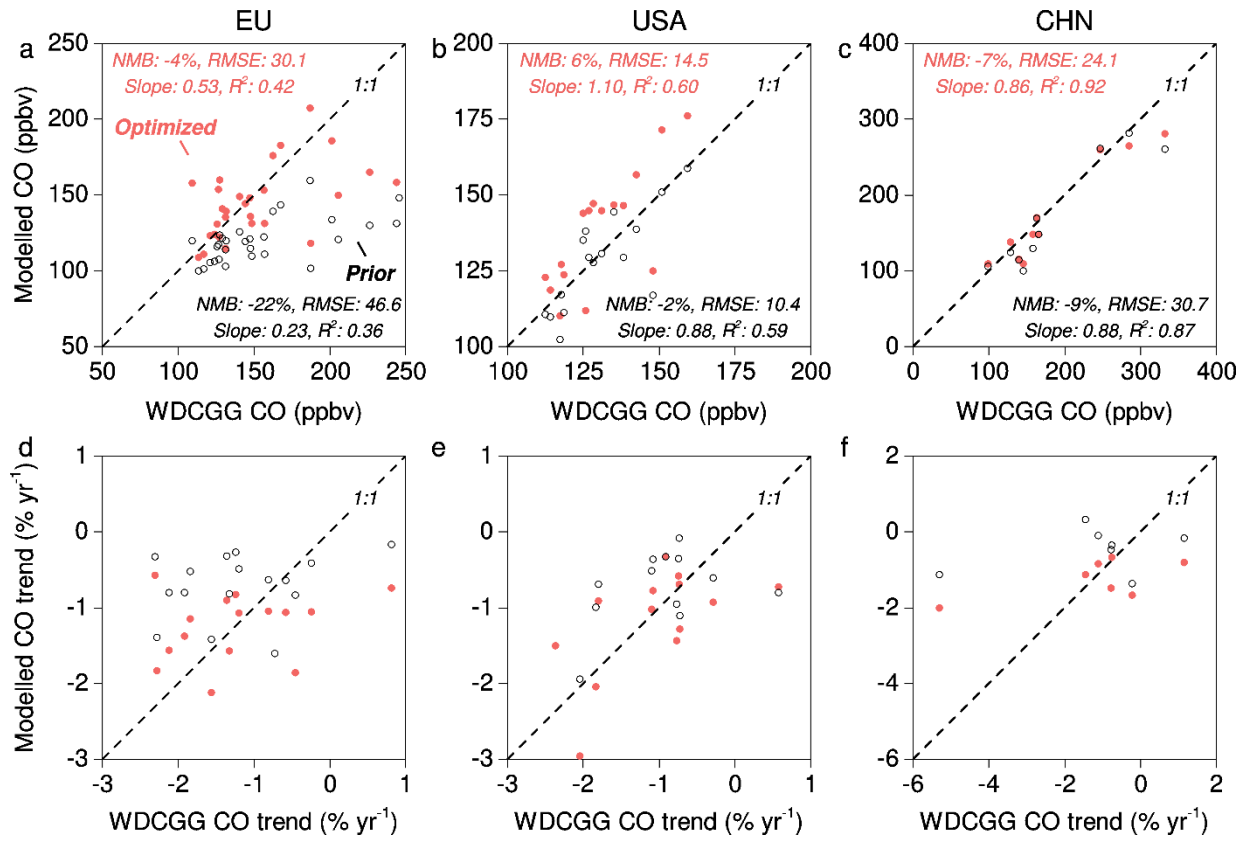


Figure S8. Evaluation of Inversion #2 with the WDCGG observations by region. The comparison is conducted for annual average and 2005–2017 trends of surface CO concentrations between the modelled results and the WDCGG observations in EU (a, d), the USA (b, e), and CHN (c, f). The WDCGG sites used for each region are within the three black boxes shown in Fig. A1. The trends are calculated based on monthly time series using a curve fitting method as described in Zheng et al. (2018).

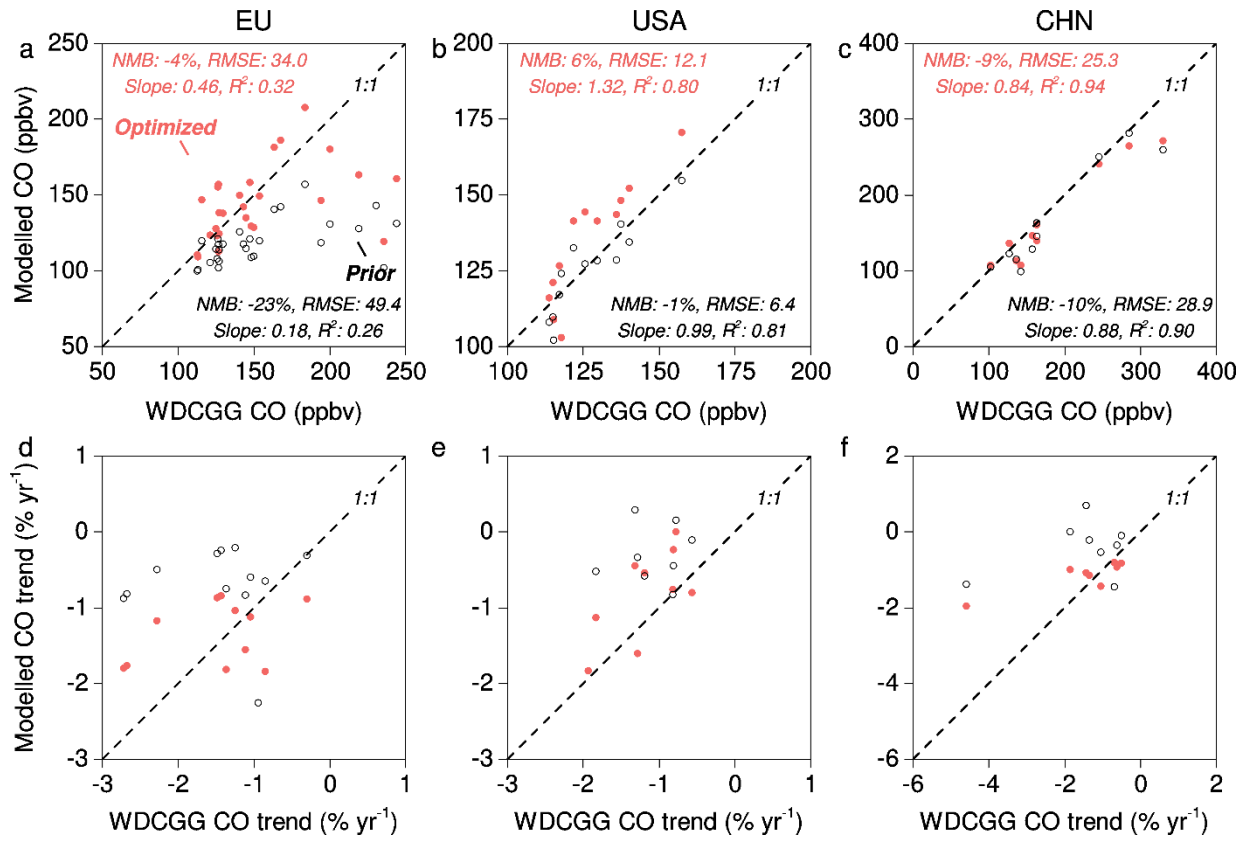


Figure S9. Evaluation of Inversion #3 with the WDCGG observations by region. The comparison is conducted for annual average and 2010–2017 trends of surface CO concentrations between the modelled results and the WDCGG observations in EU (a, d), the USA (b, e), and CHN (c, f). The WDCGG sites used for each region are within the three black boxes shown in Fig. A1. The trends are calculated based on monthly time series using a curve fitting method as described in Zheng et al. (2018).

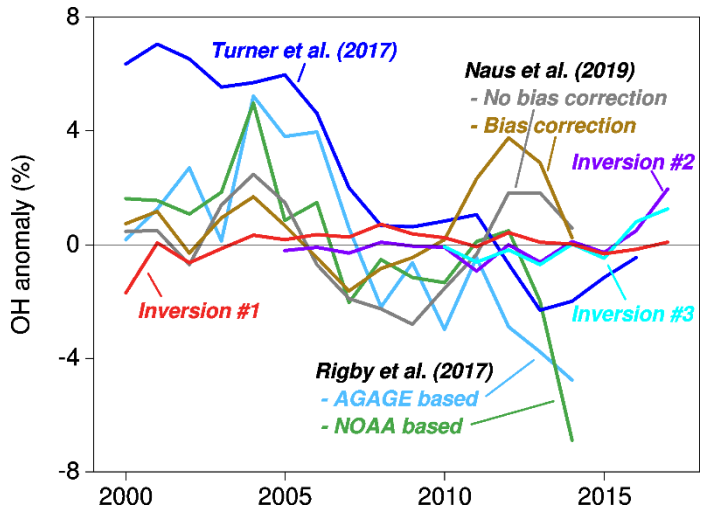


Figure S10. Comparison of OH anomalies between this study estimates and two-box model inversions from literature. This study estimates are derived from Inversion #1 (red curve), Inversion #2 (purple curve), and Inversion #3 (cyan curve). Two-box model inversions are obtained from Turner et al. (2017) (dark blue curve), Rigby et al. (2017) (light blue and green curves), and Naus et al. 5 (grey and brown curves).

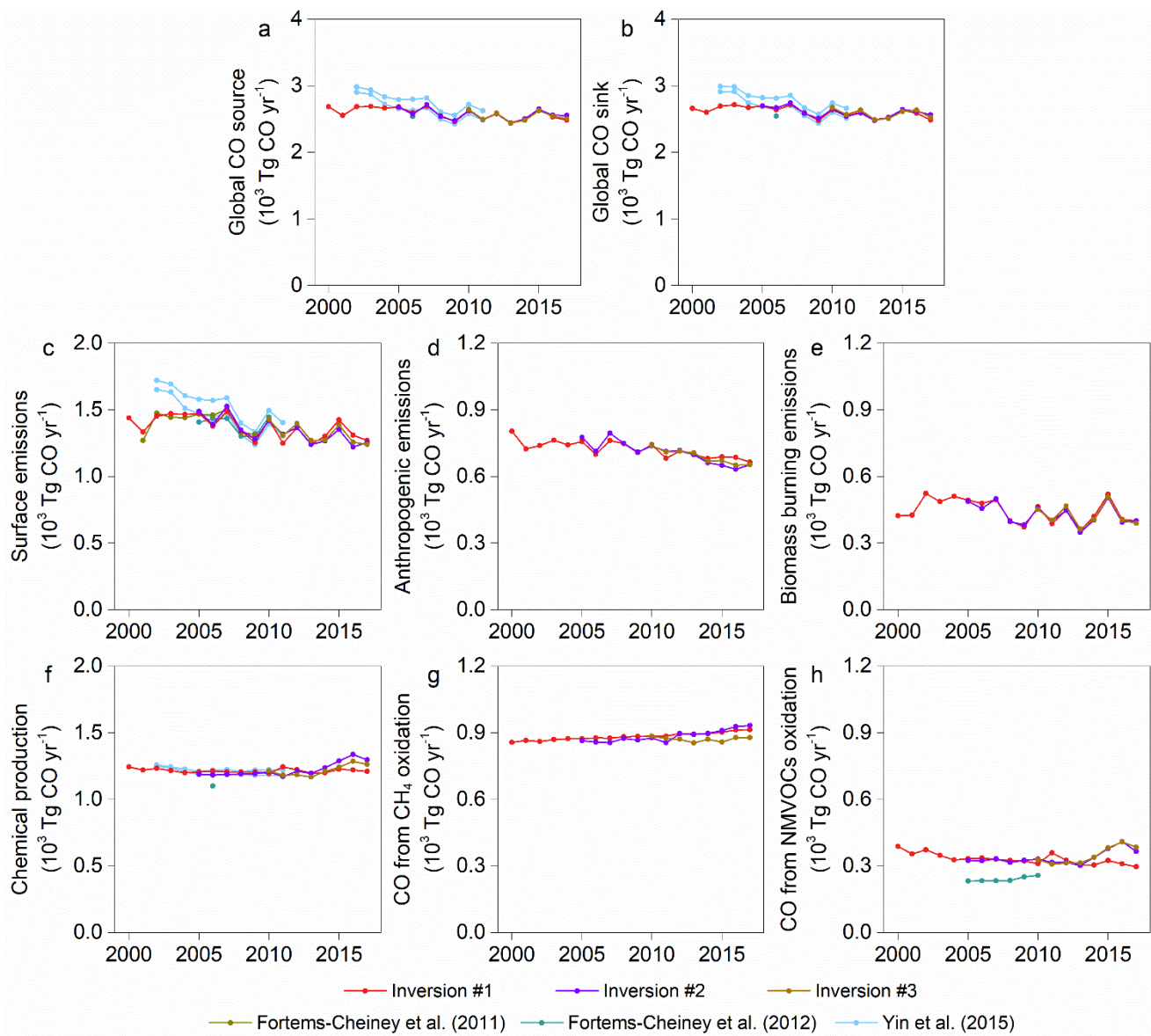


Figure S11. Comparison of Inversions #1, #2, and #3 results with the estimates using previous versions of our inversion system. The comparison is conducted for the global CO source (a), the global CO sink (b), the surface direct emissions (c), the anthropogenic emissions (d), the biomass burning emissions (e), the CO chemical production (f), the CO production from CH₄ oxidation (g), and the CO production from NMVOCs oxidation (h).

5

References

- Arellano Jr., A. F., Kasibhatla, P. S., Giglio, L., van der Werf, G. R., and Randerson, J. T.: Top-down estimates of global CO sources using MOPITT measurements, *Geophys. Res. Lett.*, 31, doi: 10.1029/2003GL018609, 2004.
- Arellano Jr., A. F., Kasibhatla, P. S., Giglio, L., van der Werf, G. R., Randerson, J. T., and Collatz, G. J.: Time-dependent inversion estimates of global biomass-burning CO emissions using Measurement of Pollution in the Troposphere (MOPITT) measurements, *J. Geophys. Res. Atmos.*, 111, doi: 10.1029/2005JD006613, 2006.
- Blumenstock, T., Hase, F., Schneider, M., García, O. E. and Sepúlveda, E.: TCCON data from Izana (ES), Release GGG2014.R1, doi:10.14291/tccon.ggg2014.izana01.r1, 2017.
- De Mazière, M., Sha, M. K., Desmet, F., Hermans, C., Scolas, F., Kumps, N., Metzger, J.-M., Duflot, V. and Cammas, J.-P.: TCCON data from Réunion Island (RE), Release GGG2014.R1, doi:10.14291/tccon.ggg2014.reunion01.r1, 2017.
- Deutscher, N. M., Notholt, J., Messerschmidt, J., Weinzierl, C., Warneke, T., Petri, C. and Grupe, P.: TCCON data from Bialystok (PL), Release GGG2014.R1, doi:10.14291/tccon.ggg2014.bialystok01.r1/1183984, 2017.
- Dubey, M. K., Henderson, B. G., Green, D., Butterfield, Z. T., Keppel-Aleks, G., Allen, N. T., Blavier, J.-F., Roehl, C. M., Wunch, D. and Lindenmaier, R.: TCCON data from Manaus (BR), Release GGG2014.R0, doi:10.14291/tccon.ggg2014.manaus01.r0/1149274, 2017a.
- Dubey, M. K., Lindenmaier, R., Henderson, B. G., Green, D., Allen, N. T., Roehl, C. M., Blavier, J.-F., Butterfield, Z. T., Love, S., Hamelmann, J. D. and Wunch, D.: TCCON data from Four Corners (US), Release GGG2014.R0, doi:10.14291/tccon.ggg2014.fourcorners01.r0/1149272, 2017b.
- Feist, D. G., Arnold, S. G., John, N. and Geibel, M. C.: TCCON data from Ascension Island (SH), Release GGG2014.R0, doi:10.14291/tccon.ggg2014.ascending01.r0/1149285, 2017.
- Fortems-Cheiney, A., Chevallier, F., Pison, I., Bousquet, P., Szopa, S., Deeter, M. N., and Clerbaux, C.: Ten years of CO emissions as seen from Measurements of Pollution in the Troposphere (MOPITT), *J. Geophys. Res. Atmos.*, 116, D05304, doi: 10.1029/2010JD014416, 2011.
- Fortems-Cheiney, A., Chevallier, F., Pison, I., Bousquet, P., Saunois, M., Szopa, S., Cressot, C., Kurosu, T. P., Chance, K., and Fried, A.: The formaldehyde budget as seen by a global-scale multi-constraint and multi-species inversion system, *Atmos. Chem. Phys.*, 12, 6699-6721, doi: 10.5194/acp-12-6699-2012, 2012.
- Gaubert, B., Worden, H. M., Arellano, A. F. J., Emmons, L. K., Tilmes, S., Barré, J., Martinez Alonso, S., Vitt, F., Anderson, J. L., Alkemade, F., Houweling, S., and Edwards, D. P.: Chemical Feedback From Decreasing Carbon Monoxide Emissions, *Geophys. Res. Lett.*, 44, 9985-9995, doi: 10.1002/2017GL074987, 2017.
- Goo, T.-Y., Oh, Y.-S. and Velazco, V. A.: TCCON data from Anmeyondo (KR), Release GGG2014.R0, doi:10.14291/tccon.ggg2014.anmeyondo01.r0/1149284, 2017.

- Griffith, D. W. T., Velazco, V. A., Deutscher, N. M., Paton-Walsh, C., Jones, N. B., Wilson, S. R., Macatangay, R. C., Kettlewell, G. C., Buchholz, R. R. and Rigenbach, M. O.: TCCON data from Wollongong (AU), Release GGG2014.R0, doi:10.14291/tcccon.ggg2014.wollongong01.r0/1149291, 2017a.
- Griffith, D. W. T., Deutscher, N. M., Velazco, V. A., Wennberg, P. O., Yavin, Y., Keppel-Aleks, G., Washenfelder, R. A.,
5 Toon, G. C., Blavier, J.-F., Paton-Walsh, C., Jones, N. B., Kettlewell, G. C., Connor, B. J., Macatangay, R. C., Roehl, C., Ryczek, M., Glowacki, J., Culgan, T. and Bryant, G. W.: TCCON data from Darwin (AU), Release GGG2014.R0, doi:10.14291/tcccon.ggg2014.darwin01.r0/1149290, 2017b.
- Hase, F., Blumenstock, T., Dohe, S., Groß, J. and Kiel, M. ä.: TCCON data from Karlsruhe (DE), Release GGG2014.R1, doi:10.14291/tcccon.ggg2014.karlsruhe01.r1/1182416, 2017.
- 10 Iraci, L. T., Podolske, J. R., Hillyard, P. W., Roehl, C., Wennberg, P. O., Blavier, J.-F., Landeros, J., Allen, N., Wunch, D., Zavaleta, J., Quigley, E., Osterman, G. B., Barrow, E. and Barney, J.: TCCON data from Indianapolis (US), Release GGG2014.R1, doi:10.14291/tcccon.ggg2014.indianapolis01.r1/1330094, 2017a.
- Iraci, L. T., Podolske, J. R., Hillyard, P. W., Roehl, C., Wennberg, P. O., Blavier, J.-F., Landeros, J., Allen, N., Wunch, D., Zavaleta, J., Quigley, E., Osterman, G. B., Albertson, R., Dunwoody, K. and Boyden, H.: TCCON data from Edwards (US),
15 Release GGG2014.R1, doi:10.14291/tcccon.ggg2014.edwards01.r1/1255068, 2017b.
- Jiang, Z., Worden, J. R., Worden, H., Deeter, M., Jones, D. B. A., Arellano, A. F., and Henze, D. K.: A 15-year record of CO emissions constrained by MOPITT CO observations, *Atmos. Chem. Phys.*, 17, 4565-4583, doi: 10.5194/acp-17-4565-2017, 2017.
- Kawakami, S., Ohyama, H., Arai, K., Okumura, H., Taura, C., Fukamachi, T. and Sakashita, M.: TCCON data from Saga
20 (JP), Release GGG2014.R0, doi:10.14291/tcccon.ggg2014.saga01.r0/1149283, 2017.
- Kivi, R., Heikkinen, P. and Kyrö, E.: TCCON data from Sodankylä (FI), Release GGG2014.R0, doi:10.14291/tcccon.ggg2014.sodankyla01.r0/1149280, 2017.
- Kopacz, M., Jacob, D. J., Fisher, J. A., Logan, J. A., Zhang, L., Megretskaya, I. A., Yantosca, R. M., Singh, K., Henze, D. K., Burrows, J. P., Buchwitz, M., Khlystova, I., McMillan, W. W., Gille, J. C., Edwards, D. P., Eldering, A., Thouret, V., and
25 Nedelec, P.: Global estimates of CO sources with high resolution by adjoint inversion of multiple satellite datasets (MOPITT, AIRS, SCIAMACHY, TES), *Atmos. Chem. Phys.*, 10, 855-876, doi: 10.5194/acp-10-855-2010, 2010.
- Morino, I., Yokozeki, N., Matsuzaki, T. and Horikawa, M.: TCCON data from Rikubetsu (JP), Release GGG2014.R2, , doi:10.14291/tcccon.ggg2014.rikubetsu01.r2, 2017a.
- Morino, I., Matsuzaki, T. and Horikawa, M.: TCCON data from Tsukuba (JP), 125HR, Release GGG2014.R2,
30 doi:10.14291/tcccon.ggg2014.tsukuba02.r2, 2017b.
- Morino, I., Velazco, V. A., Hori, A., Uchino, O. and Griffith, D. W. T.: TCCON data from Burgos, Ilocos Norte (PH), Release GGG2014.R0, doi:10.14291/tcccon.ggg2014.burgos01.r0, 2018.

- Müller, J.-F., Stavrakou, T., Bauwens, M., George, M., Hurtmans, D., Coheur, P.-F., Clerbaux, C., and Sweeney, C.: Top-Down CO Emissions Based On IASI Observations and Hemispheric Constraints on OH Levels, *Geophys. Res. Lett.*, 45, 1621-1629, doi:10.1002/2017GL076697, 2018.
- Notholt, J., Warneke, T., Petri, C., Deutscher, N. M., Weinzierl, C., Palm, M. and Buschmann, M.: TCCON data from Ny Ålesund, Spitsbergen (NO), Release GGG2014.R0, doi:10.14291/tccon.ggg2014.nyalesund01.r0/1149278, 2017a.
- Notholt, J., Petri, C., Warneke, T., Deutscher, N. M., Palm, M., Buschmann, M., Weinzierl, C., Macatangay, R. C. and Grupe, P.: TCCON data from Bremen (DE), Release GGG2014.R0, doi:10.14291/tccon.ggg2014.bremen01.r0/1149275, 2017b.
- Park, K., Emmons, L. K., Wang, Z., and Mak, J. E.: Joint Application of Concentration and $\delta^{18}\text{O}$ to Investigate the Global Atmospheric CO Budget, *Atmosphere*, 6, 547, 2015.
- Pétron, G., Granier, C., Khattatov, B., Yudin, V., Lamarque, J.-F., Emmons, L., Gille, J., and Edwards, D. P.: Monthly CO surface sources inventory based on the 2000–2001 MOPITT satellite data, *Geophys. Res. Lett.*, 31, n/a-n/a, doi: 10.1029/2004GL020560, 2004.
- Rigby, M., Montzka, S. A., Prinn, R. G., White, J. W. C., Young, D., O'Doherty, S., Lunt, M. F., Ganesan, A. L., Manning, A. J., Simmonds, P. G., Salameh, P. K., Harth, C. M., Mühle, J., Weiss, R. F., Fraser, P. J., Steele, L. P., Krummel, P. B., McCulloch, A., and Park, S.: Role of atmospheric oxidation in recent methane growth, *Proc. Natl. Acad. Sci.*, 114, 5373, doi: 10.1073/pnas.1616426114, 2017.
- Naus, S., Montzka, S. A., Pandey, S., Basu, S., Dlugokencky, E. J., and Krol, M.: Constraints and biases in a tropospheric two-box model of OH, *Atmos. Chem. Phys.*, 19, 407-424, doi: 10.5194/acp-19-407-2019, 2019.
- Sherlock, V., Connor, B., Robinson, J., Shiona, H., Smale, D. and Pollard, D. F.: TCCON data from Lauder (NZ), 120HR, Release GGG2014.R0, doi:10.14291/tccon.ggg2014.lauder01.r0/1149293, 2017a.
- Sherlock, V., Connor, B., Robinson, J., Shiona, H., Smale, D. and Pollard, D. F.: TCCON data from Lauder (NZ), 125HR, Release GGG2014.R0, doi:10.14291/tccon.ggg2014.lauder02.r0/1149298, 2017b.
- Stavrakou, T., and Müller, J.-F.: Grid-based versus big region approach for inverting CO emissions using Measurement of Pollution in the Troposphere (MOPITT) data, *J. Geophys. Res. Atmos.*, 111, doi: 10.1029/2005JD006896, 2006.
- Strong, K., Roche, S., Franklin, J. E., Mendonca, J., Lutsch, E., Weaver, D., Fogal, P. F., Drummond, J. R., Batchelor, R. and Lindenmaier, R.: TCCON data from Eureka (CA), Release GGG2014.R3, doi:10.14291/tccon.ggg2014.eureka01.r3, 2018.
- Sussmann, R. and Rettinger, M.: TCCON data from Garmisch (DE), Release GGG2014.R2, doi:10.14291/tccon.ggg2014.garmisch01.r2, 2017.
- Sussmann, R. and Rettinger, M.: TCCON data from Zugspitze (DE), Release GGG2014.R1, doi:10.14291/tccon.ggg2014.zugspitze01.r1, 2018.
- Té, Y., Jeseck, P. and Janssen, C.: TCCON data from Paris (FR), Release GGG2014.R0, doi:10.14291/tccon.ggg2014.paris01.r0/1149279, 2017.

- Turner, A. J., Frankenberg, C., Wennberg, P. O., and Jacob, D. J.: Ambiguity in the causes for decadal trends in atmospheric methane and hydroxyl, Proc. Natl. Acad. Sci., 114, 5367, doi: 10.1073/pnas.1616020114, 2017.
- Warneke, T., Messerschmidt, J., Notholt, J., Weinzierl, C., Deutscher, N. M., Petri, C. and Grupe, P.: TCCON data from Orléans (FR), Release GGG2014.R0, doi:10.14291/tcccon.ggg2014.orleans01.r0/1149276, 2017.
- 5 Wennberg, P. O., Wunch, D., Roehl, C. M., Blavier, J.-F., Toon, G. C. and Allen, N. T.: TCCON data from Caltech (US), Release GGG2014.R1, doi:10.14291/tcccon.ggg2014.pasadena01.r1/1182415, 2017a.
- Wennberg, P. O., Wunch, D., Yavin, Y., Toon, G. C., Blavier, J.-F., Allen, N. T. and Keppel-Aleks, G.: TCCON data from Jet Propulsion Laboratory (US), 2007, Release GGG2014.R0, doi:10.14291/tcccon.ggg2014.jpl01.r0/1149163, 2017b.
- Wennberg, P. O., Roehl, C. M., Blavier, J.-F., Wunch, D. and Allen, N. T.: TCCON data from Jet Propulsion Laboratory 10 (US), 2011, Release GGG2014.R1, doi:10.14291/tcccon.ggg2014.jpl02.r1/1330096, 2017c.
- Wennberg, P. O., Roehl, C. M., Wunch, D., Toon, G. C., Blavier, J.-F., Washenfelder, R., Keppel-Aleks, G., Allen, N. T. and Ayers, J.: TCCON data from Park Falls (US), Release GGG2014.R1, doi:10.14291/tcccon.ggg2014.parkfalls01.r1, 2017d.
- Wennberg, P. O., Wunch, D., Roehl, C. M., Blavier, J.-F., Toon, G. C. and Allen, N. T.: TCCON data from Lamont (US), 15 Release GGG2014.R1, doi:10.14291/tcccon.ggg2014.lamont01.r1/1255070, 2017e.
- Wunch, D., Mendonca, J., Colebatch, O., Allen, N. T., Blavier, J.-F., Roche, S., Hedelius, J., Neufeld, G., Springett, S., Worthy, D., Kessler, R. and Strong, K.: TCCON data from East Trout Lake, SK (CA), Release GGG2014.R1, doi:10.14291/tcccon.ggg2014.easttroutlake01.r1, 2017.
- Yin, Y., Chevallier, F., Ciais, P., Broquet, G., Fortems-Cheiney, A., Pison, I., and Saunois, M.: Decadal trends in global CO 20 emissions as seen by MOPITT, Atmos. Chem. Phys., 15, 13433-13451, doi: 10.5194/acp-15-13433-2015, 2015.
- Yin, Y., Ciais, P., Chevallier, F., van der Werf, G. R., Fanin, T., Broquet, G., Boesch, H., Cozic, A., Hauglustaine, D., Szopa, S., and Wang, Y.: Variability of fire carbon emissions in equatorial Asia and its nonlinear sensitivity to El Niño, Geophys. Res. Lett., 43, 10,472-410,479, doi: 10.1002/2016GL070971, 2016.
- Zheng, B., Chevallier, F., Ciais, P., Yin, Y., Deeter, M., Worden, H., Wang, Y. L., Zhang, Q., and He, K. B.: Rapid decline 25 in carbon monoxide emissions and export from East Asia between years 2005 and 2016, Environ. Res. Lett., 13, 044007, doi: 10.1088/1748-9326/aab2b3, 2018.